3.1 What is turbulence?

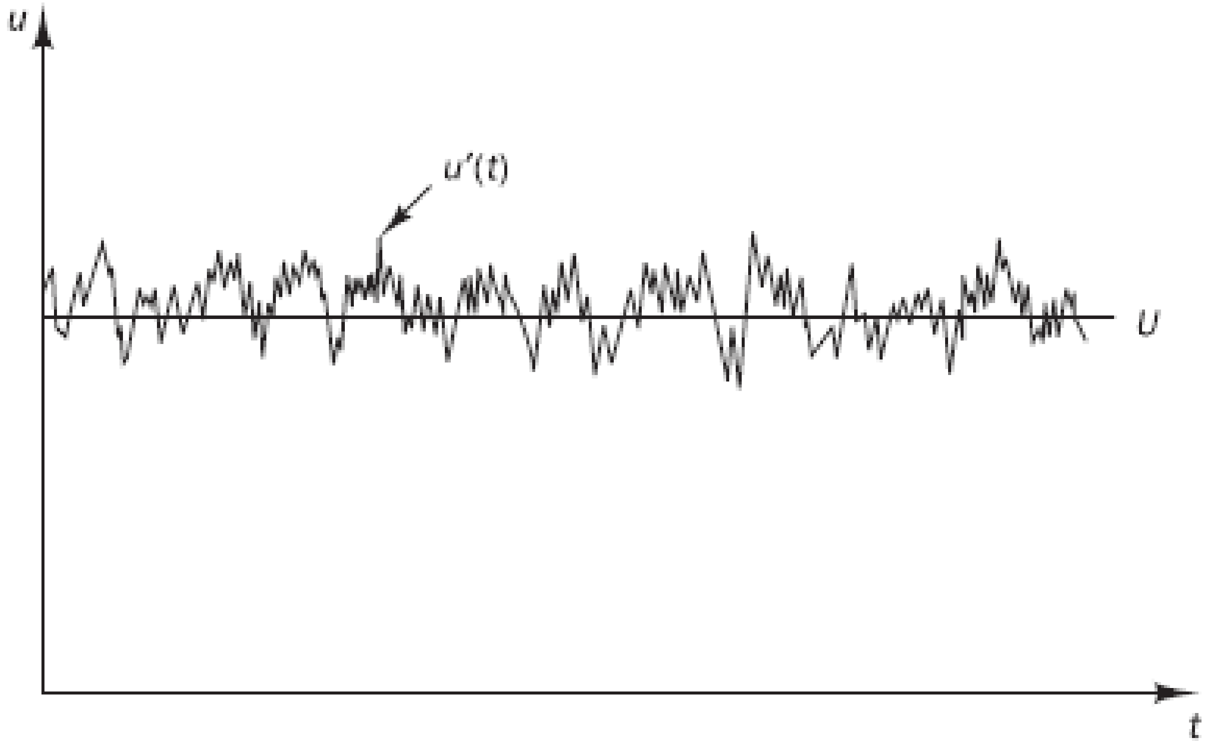

Figure 3.2 Visualisation of a turbulent boundary layer
Source: Van Dyke (1982)

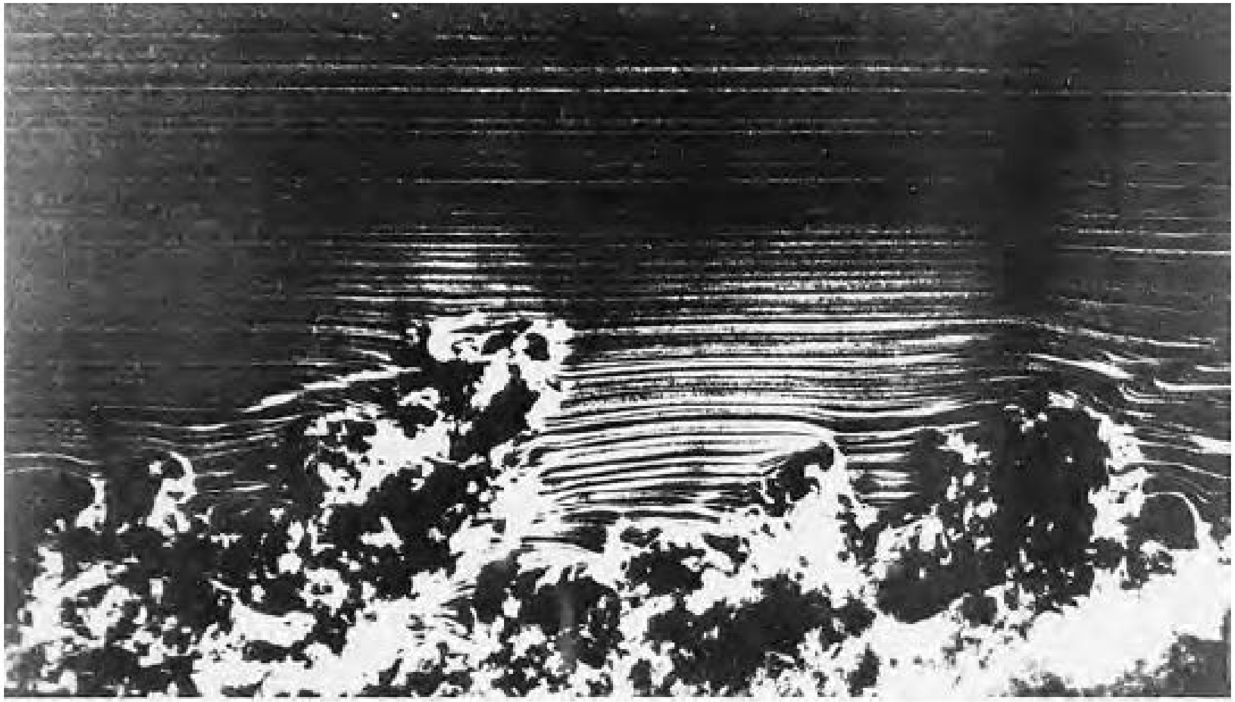

Figure 3.3 Energy spectrum of turbulence behind a grid

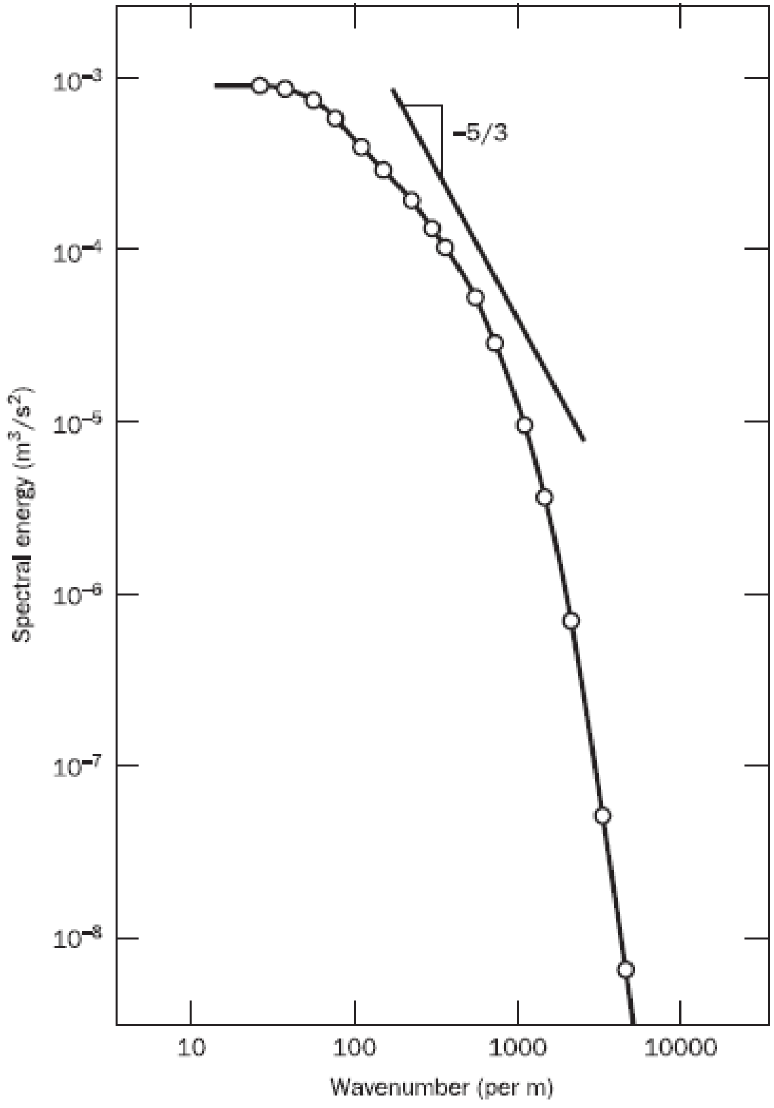

Figure 3.4 Velocity profiles susceptible to (a) inviscid instability and (b) viscous instability

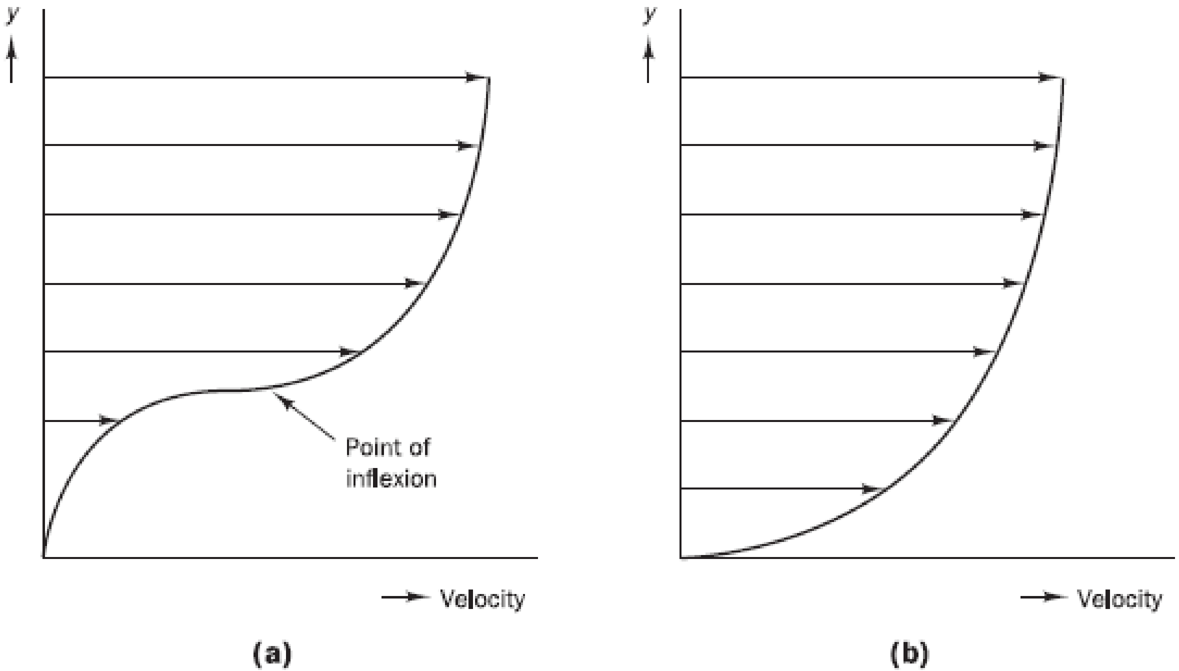

Figure 3.5 Transition in a jet flow

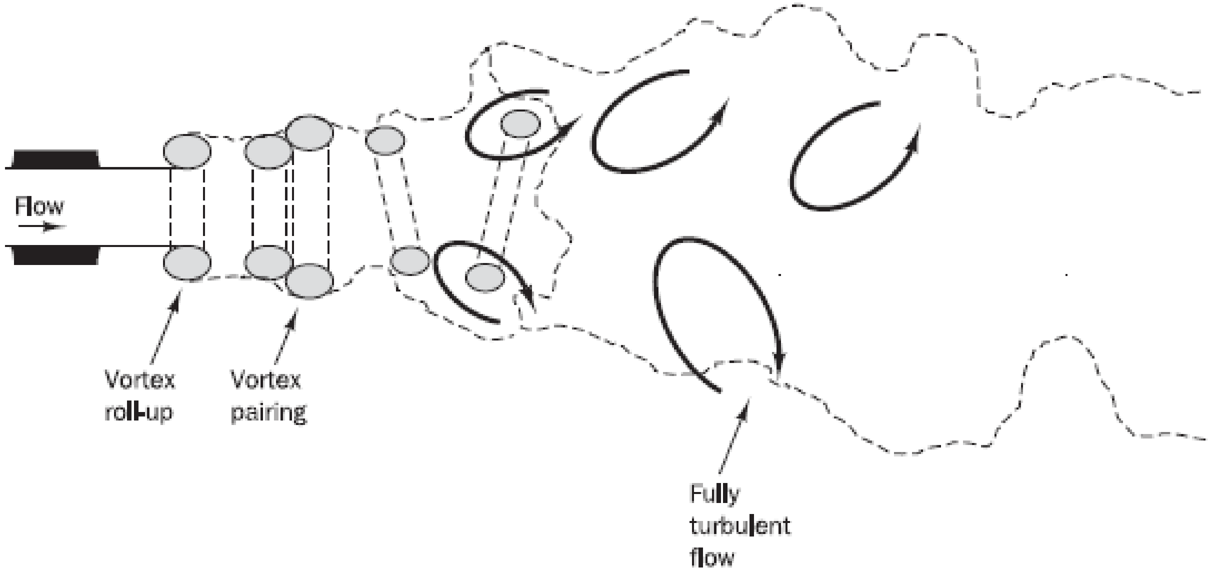

Figure 3.6 Plan view sketch of transition processes in boundary layer flow over a flat plate

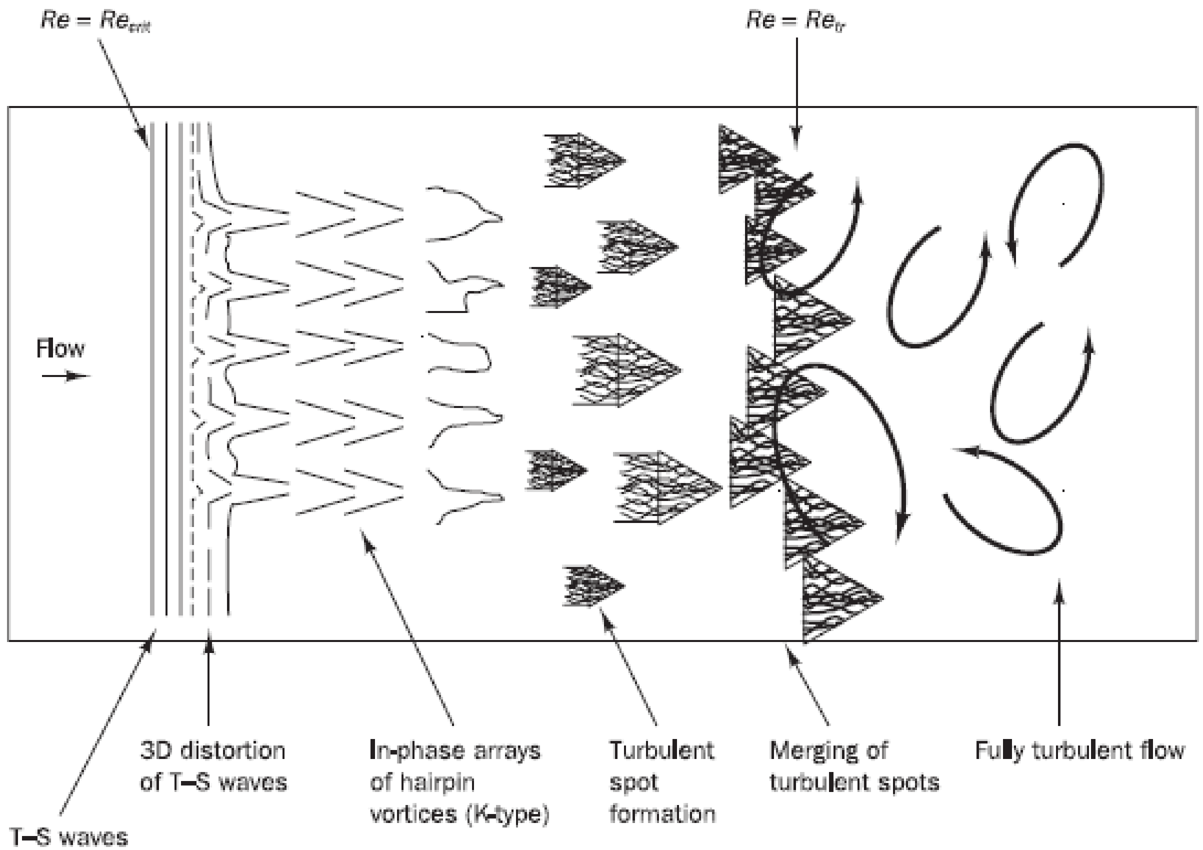

Figure 3.7 Merging of turbulent spots and transition to turbulence in a flat plate boundary layer
Source: Nakayama (1988)

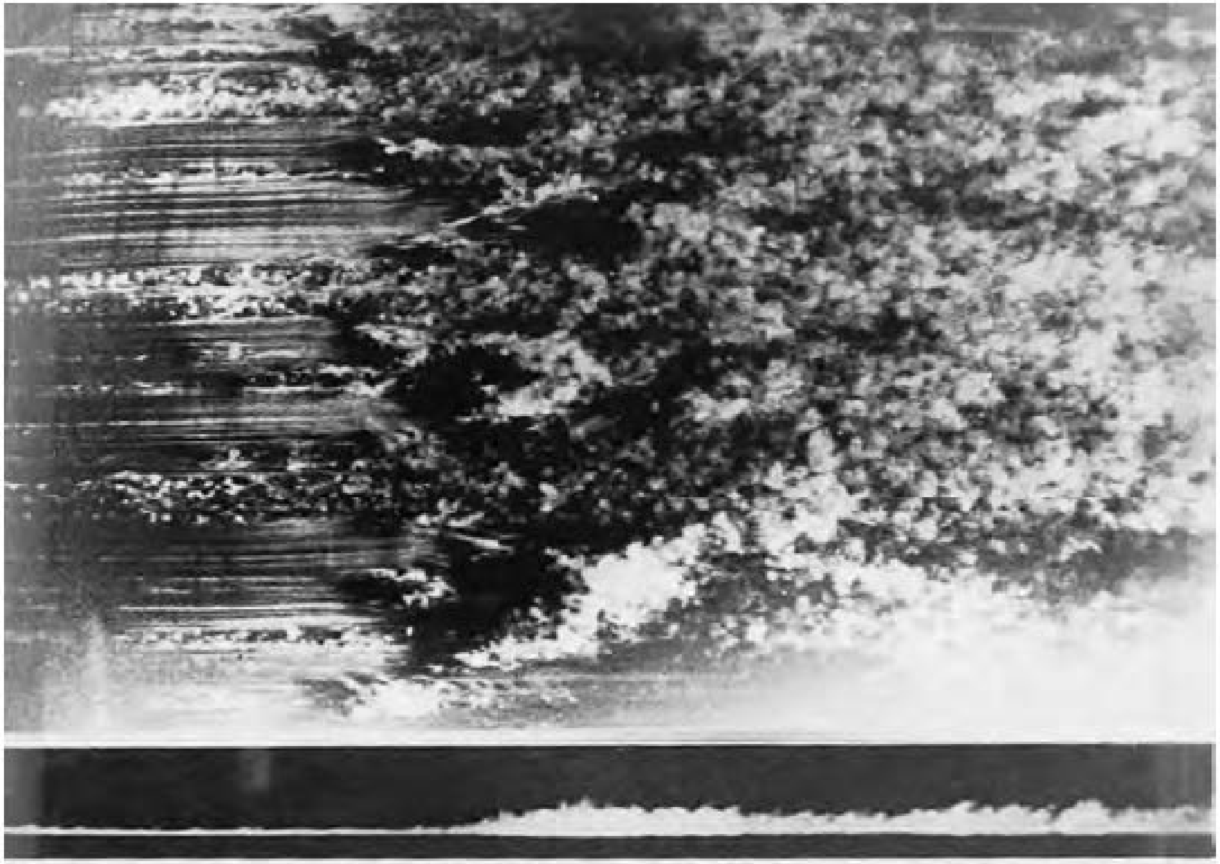

3.4 Characteristics of simple turbulent flows

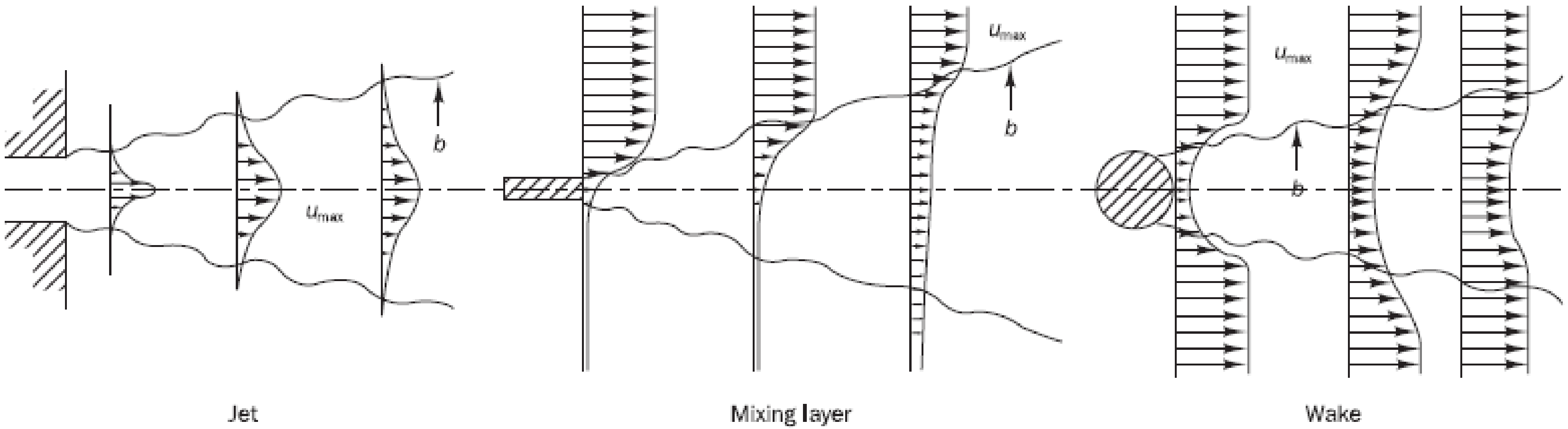

Figure 3.8 Free turbulent flows

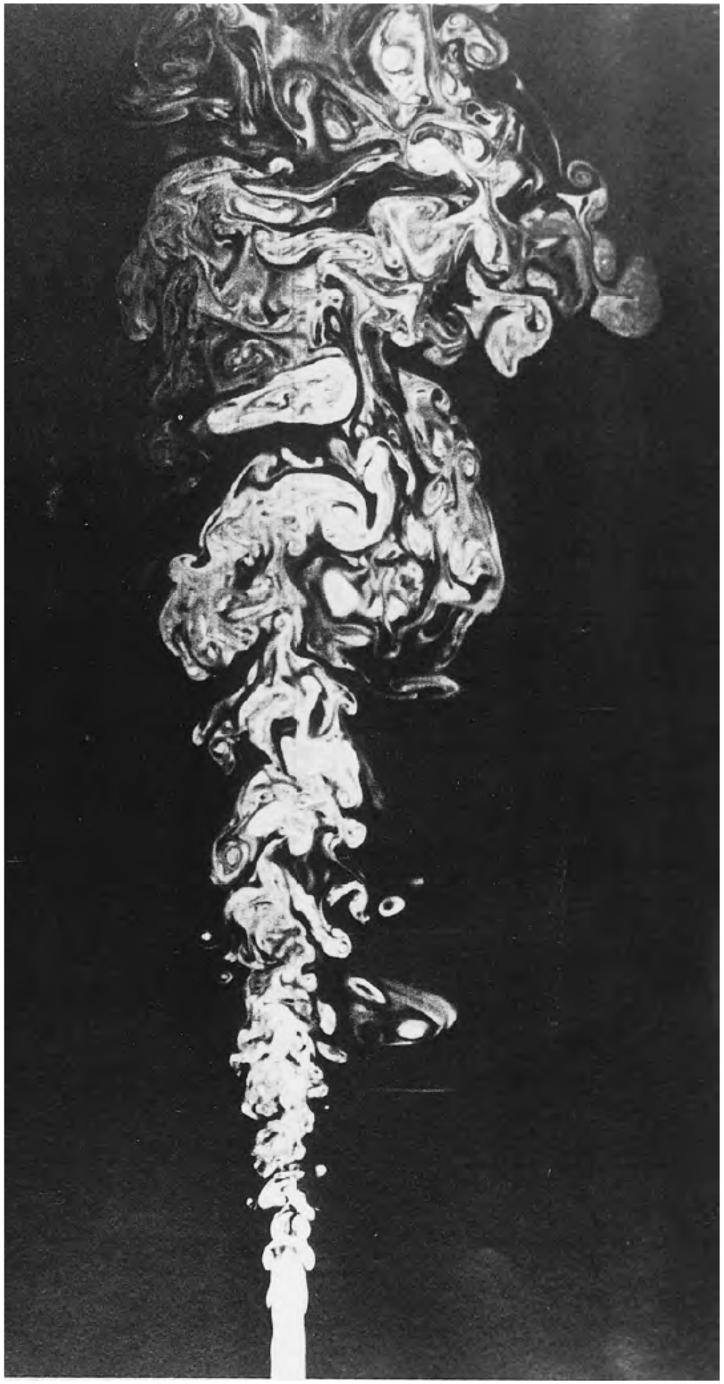

Figure 3.10 Distribution of mean velocity and second moments $\overline{u'^2}$, $\overline{v'^2}$, $\overline{w'^2}$ and $-\overline{u'v'}$ for incompressible mixing layer, jet and wake

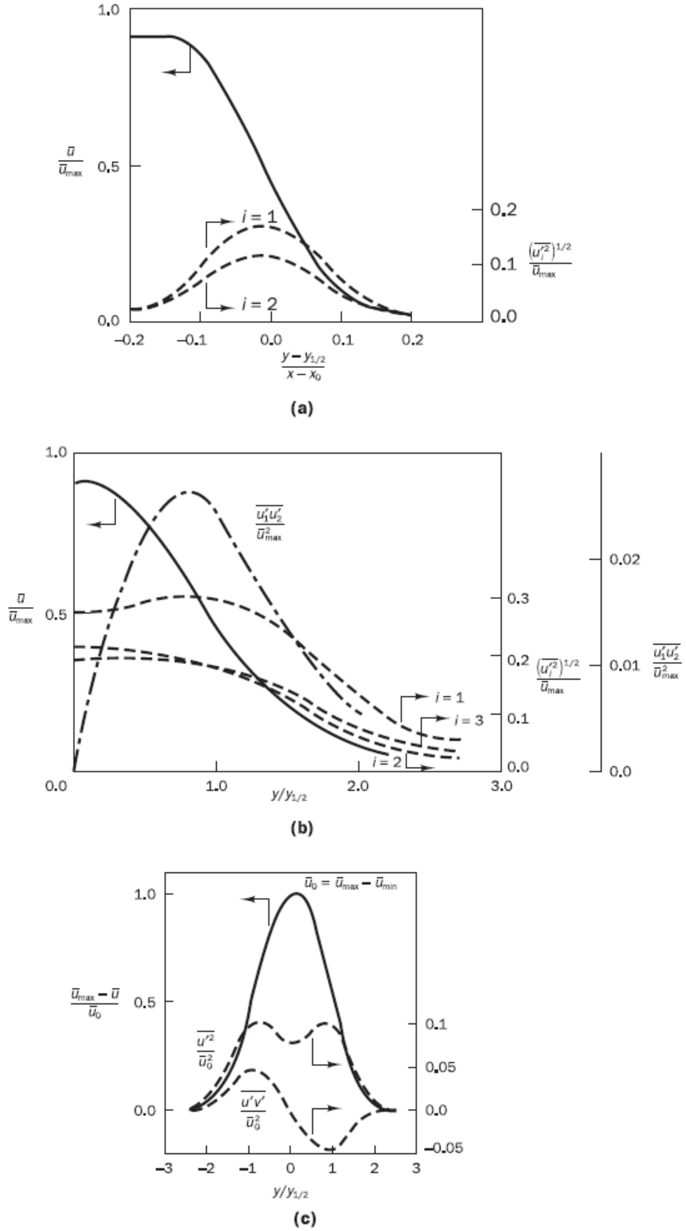

Figure 3.11 Velocity distribution near a solid wall *Source*: Schlichting, H. (1979) *Boundary Layer Theory*, 7th edn, reproduced with permission of The McGraw-Hill Companies

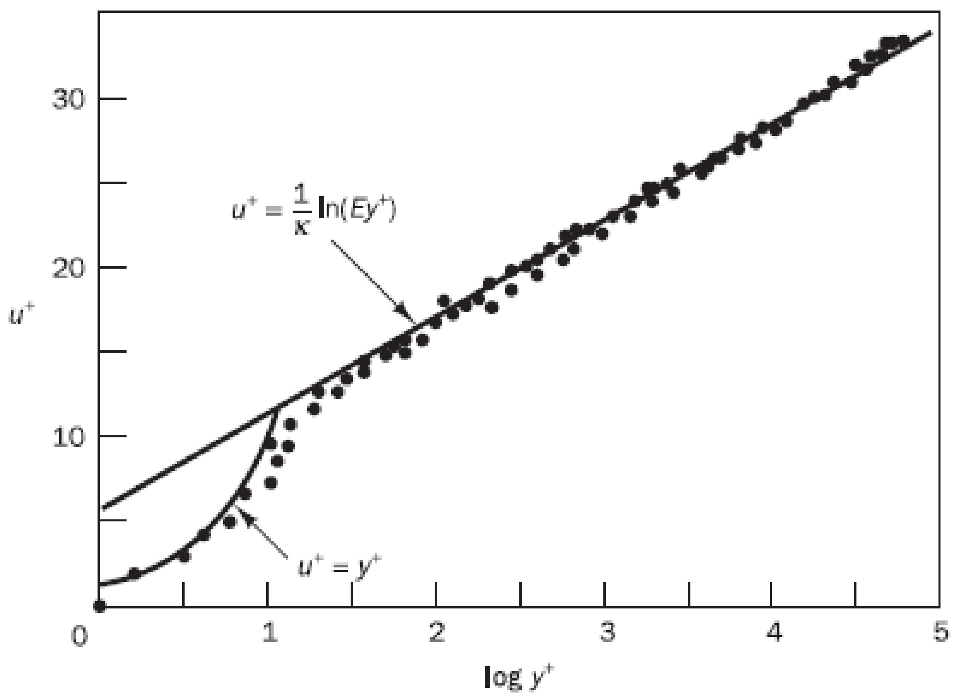

Figure 3.12 Distribution of mean velocity and second moments $\overline{u'^2}$, $\overline{v'^2}$, $\overline{w'^2}$ and $-\overline{u'v'}$ for flat plate boundary layer

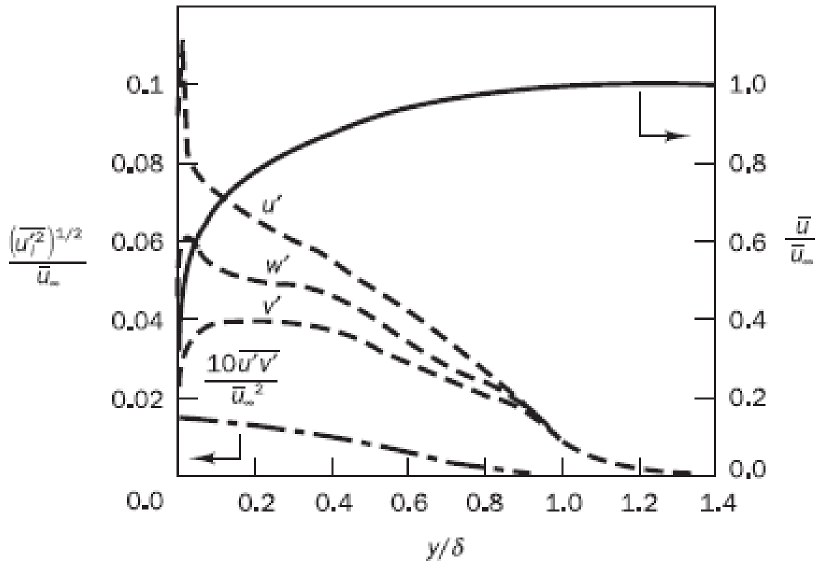

3.5 The effect of turbulent fluctuations on properties of the mean flow

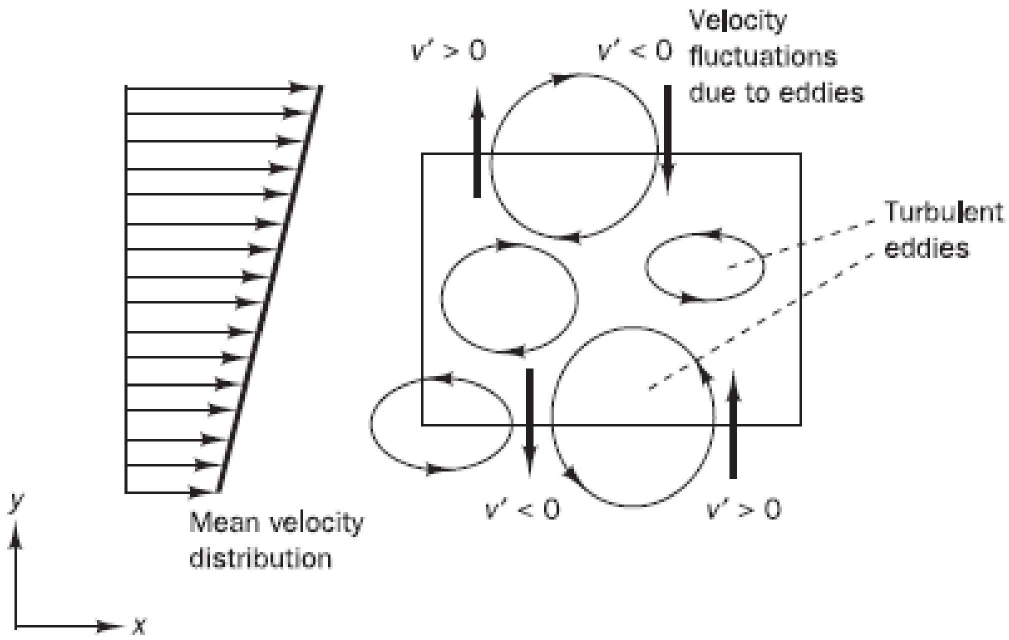

Table 3.1 Turbulent flow equations for compressible flows

Continuity $\frac{\partial \bar{\rho}}{\partial t} + \mathrm{div}(\bar{\rho}\tilde{\mathbf{U}}) = 0$ (3.30)

Reynolds equations

$$\frac{\partial(\bar{\rho}\tilde{U})}{\partial t} + \mathrm{div}(\bar{\rho}\tilde{U}\tilde{\mathbf{U}}) = -\frac{\partial \bar{P}}{\partial x} + \mathrm{div}(\mu \text{ grad } \tilde{U}) + \left[-\frac{\partial(\overline{\bar{\rho}u'^2})}{\partial x} - \frac{\partial(\overline{\bar{\rho}u'v'})}{\partial y} - \frac{\partial(\overline{\bar{\rho}u'w'})}{\partial z}\right] + S_{Mx} \quad (3.31a)$$

$$\frac{\partial(\bar{\rho}\tilde{V})}{\partial t} + \mathrm{div}(\bar{\rho}\tilde{V}\tilde{\mathbf{U}}) = -\frac{\partial \bar{P}}{\partial y} + \mathrm{div}(\mu \text{ grad } \tilde{V}) + \left[-\frac{\partial(\overline{\bar{\rho}u'v'})}{\partial x} - \frac{\partial(\overline{\bar{\rho}v'^2})}{\partial y} - \frac{\partial(\overline{\bar{\rho}v'w'})}{\partial z}\right] + S_{My} \quad (3.31b)$$

$$\frac{\partial(\bar{\rho}\tilde{W})}{\partial t} + \mathrm{div}(\bar{\rho}\tilde{W}\tilde{\mathbf{U}}) = -\frac{\partial \bar{P}}{\partial z} + \mathrm{div}(\mu \text{ grad } \tilde{W}) + \left[-\frac{\partial(\overline{\bar{\rho}u'w'})}{\partial x} - \frac{\partial(\overline{\bar{\rho}v'w'})}{\partial y} - \frac{\partial(\overline{\bar{\rho}w'^2})}{\partial z}\right] + S_{Mz} \quad (3.31c)$$

Scalar transport equation

$$\frac{\partial(\bar{\rho}\tilde{\Phi})}{\partial t} + \mathrm{div}(\bar{\rho}\tilde{\Phi}\tilde{\mathbf{U}}) = \mathrm{div}(\Gamma_{\Phi} \text{ grad } \tilde{\Phi}) + \left[-\frac{\partial(\overline{\bar{\rho}u'\varphi'})}{\partial x} - \frac{\partial(\overline{\bar{\rho}v'\varphi'})}{\partial y} - \frac{\partial(\overline{\bar{\rho}w'\varphi'})}{\partial z}\right] + S_{\Phi} \quad (3.32)$$

where the overbar indicates a time-averaged variable and the tilde indicates a density-weighted or Favre-averaged variable

3.7 Reynolds-averaged Navier–Stokes equations and classical turbulence models

No. of extra transport equations	*Name*
Zero	Mixing length model
One	Spalart–Allmaras model
Two	k–ε model
	k–ω model
	Algebraic stress model
Seven	Reynolds stress model

Figure 3.14 Results of calculations using mixing length model for (a) planar jet and (b) wake behind a long, slender, circular cylinder
Source: Schlichting, H. (1979) *Boundary Layer Theory*, 7th edn, reproduced with permission of The McGraw-Hill Companies

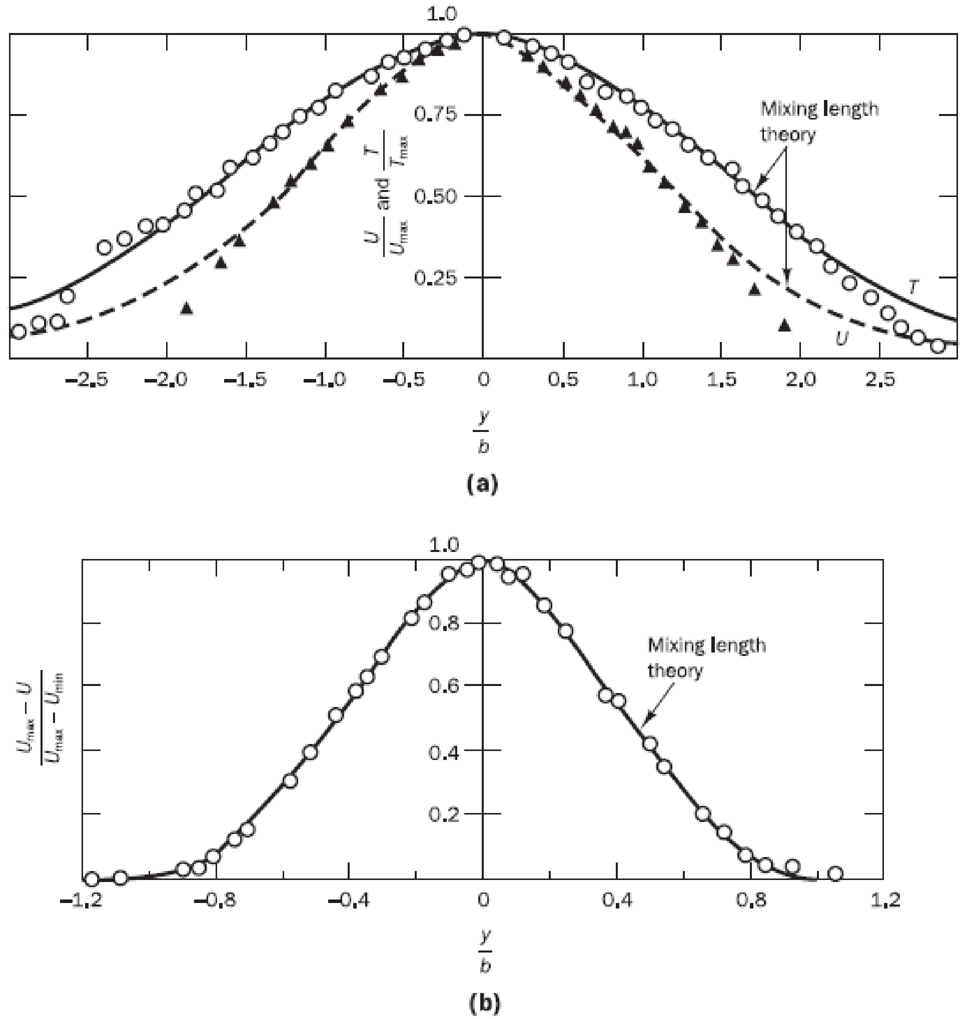

Table 3.3 Mixing length model assessment

Advantages:
- easy to implement and cheap in terms of computing resources
- good predictions for thin shear layers: jets, mixing layers, wakes and boundary layers
- well established

Disadvantages:
- completely incapable of describing flows with separation and recirculation
- only calculates mean flow properties and turbulent shear stress

Table 3.6 ASM assessment

Advantages:

- cheap method to account for Reynolds stress anisotropy
- potentially combines the generality of approach of the RSM (good modelling of buoyancy and rotation effects possible) with the economy of the k–ε model
- successfully applied to isothermal and buoyant thin shear layers
- if convection and diffusion terms are negligible the ASM performs as well as the RSM

Disadvantages:

- only slightly more expensive than the k–ε model (two PDEs and a system of algebraic equations)
- not as widely validated as the mixing length and k–ε models
- same disadvantages as RSM apply
- model is severely restricted in flows where the transport assumptions for convective and diffusive effects do not apply – validation is necessary to define performance limits

Figure 3.15 Comparison of predictions of k–ε model with measurements in an axisymmetric combustor: (a) axial velocity contours; (b) temperature contours *Source*: Jones and Whitelaw (1982)

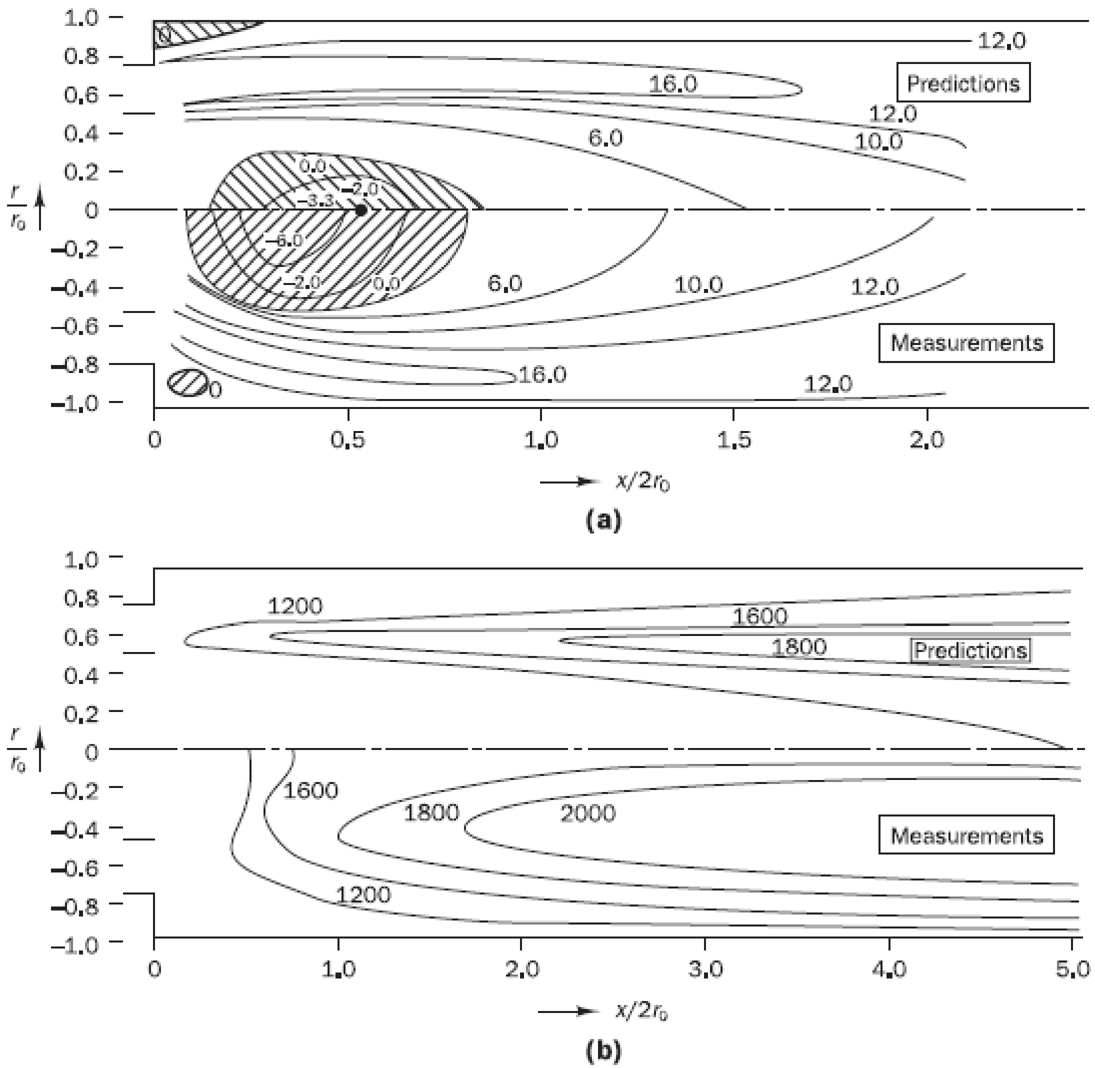

Table 3.4 Standard k–ε model assessment

Advantages:

- simplest turbulence model for which only initial and/or boundary conditions need to be supplied
- excellent performance for many industrially relevant flows
- well established, the most widely validated turbulence model

Disadvantages:

- more expensive to implement than mixing length model (two extra PDEs)
- poor performance in a variety of important cases such as:
  - (i) some unconfined flows
  - (ii) flows with large extra strains (e.g. curved boundary layers, swirling flows)
  - (iii) rotating flows
  - (iv) flows driven by anisotropy of normal Reynolds stresses (e.g. fully developed flows in non-circular ducts)

Table 3.5 RSM assessment

Advantages: • potentially the most general of all classical turbulence models • only initial and/or boundary conditions need to be supplied • very accurate calculation of mean flow properties and *all* Reynolds stresses for many simple and more complex flows including wall jets, asymmetric channel and non-circular duct flows and curved flows Disadvantages: • very large computing costs (seven extra PDEs) • not as widely validated as the mixing length and k–ε models • performs just as poorly as the k–ε model in some flows due to identical problems with the ε-equation modelling (e.g. axisymmetric jets and unconfined recirculating flows)

Figure 3.16 Comparison of predictions of RSM and standard k–ε model with measurements on a high-lift Aérospatiale aerofoil: (a) pressure coefficient; (b) skin friction coefficient
Source: Leschziner, in Peyret and Krause (2000)

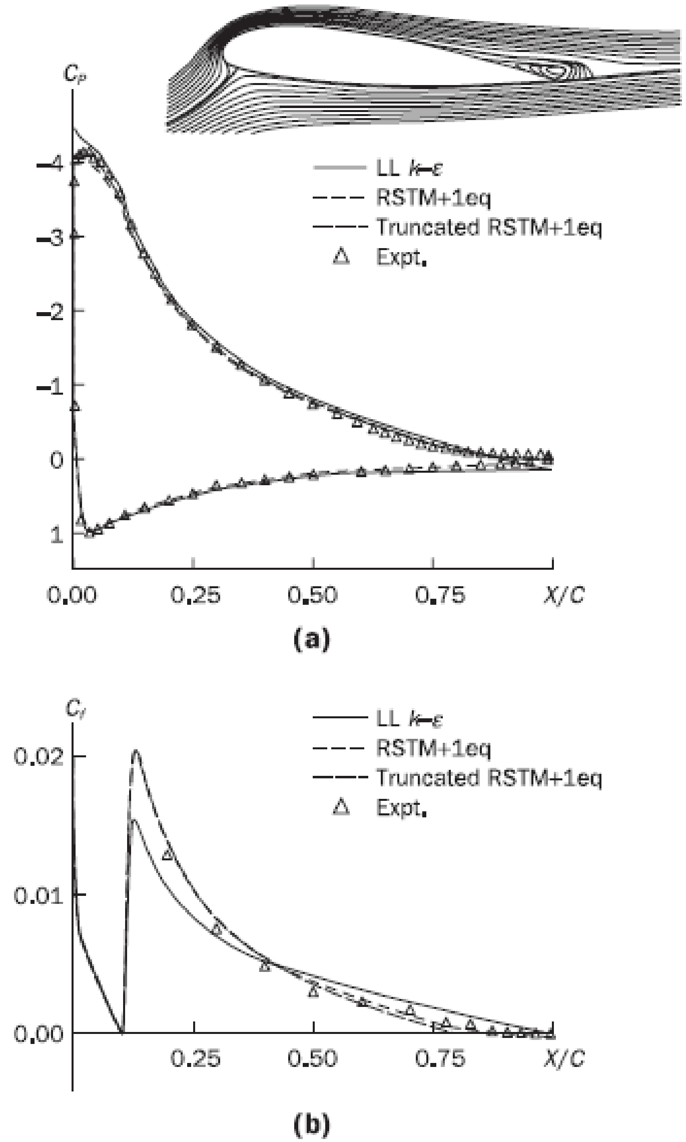

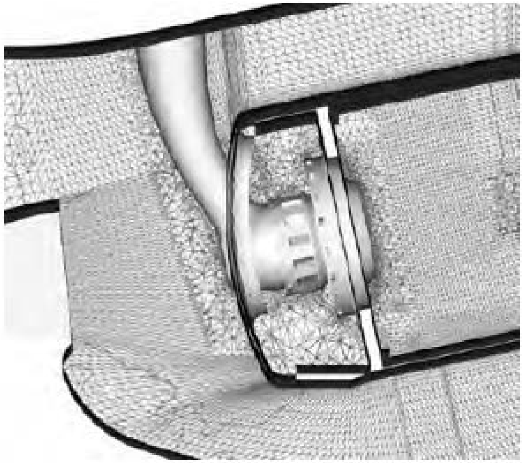

Figure 3.17 LES computations on Pratt & Whitney gas turbine – detail of combustor geometry and computational grid
Source: Moin (2002)

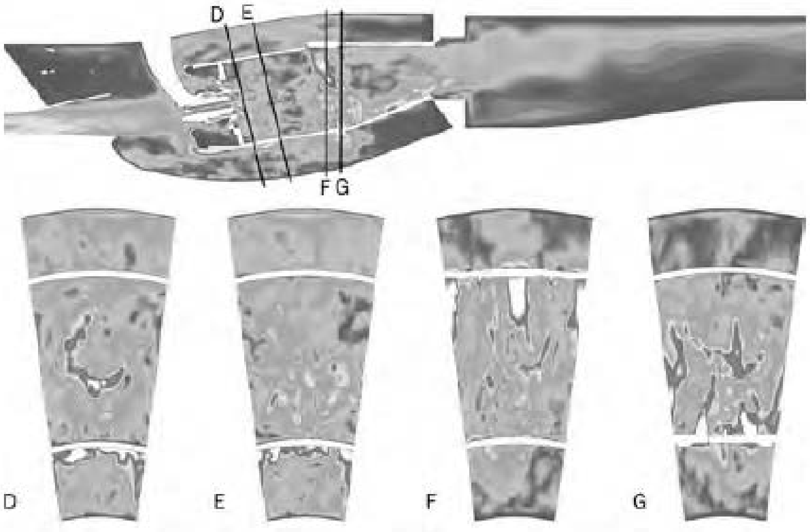

Figure 3.18 LES computations on Pratt & Whitney gas turbine – instantaneous contours of velocity magnitude on sectional planes
Source: Moin (2002)